Bone 120 (2019) 411–422

Contents lists available at ScienceDirect

Bone

journal homepage: www.elsevier.com/locate/bone

Full Length Article

Deletion of OPN in BSP knockout mice does not correct bone hypomineralization but results in high bone turnover

W. Bouleftour[a], L. Juignet[a], L. Verdière[a], I. Machuca-Gayet[b], M. Thomas[a], N. Laroche[a], A. Vanden-Bossche[a], D. Farlay[b], C. Thomas[b], E. Gineyts[b], J.P. Concordet[c], J.B. Renaud[c], D. Aubert[d], M. Teixeira[d], O. Peyruchaud[b], L. Vico[a], M.H. Lafage-Proust[a], H. Follet[b], L. Malaval[a,*]

[a] Inserm U1059-Sainbiose, Université de Lyon, F 42270 Saint Priest en Jarez, France
[b] Inserm U1033-Lyos, Université de Lyon, F69372 Lyon, France
[c] Inserm U1154/Crrs UMR7196/Muséum National d'Histoire Naturelle, F75231 Paris, France
[d] AniRa PBES, Gerland, F69007 Lyon Sud, France

ARTICLE INFO

Keywords:
SIBLING proteins
Bone sialoprotein
Osteopontin
Double knockout
Mineralization
Mouse models

ABSTRACT

The two SIBLING (Small Integrin Binding Ligand N-linked Glycoproteins), bone sialoprotein (BSP) and osteopontin (OPN) are expressed in osteoblasts and osteoclasts. In mature BSP knockout (KO, $^{-/-}$) mice, both bone formation and resorption as well as mineralization are impaired. OPN$^{-/-}$ mice display impaired resorption, and OPN is described as an inhibitor of mineralization. However, OPN is overexpressed in BSP$^{-/-}$ mice, complicating the understanding of their phenotype. We have generated and characterized mice with a double KO (DKO) of OPN and BSP, to try and unravel their respective contributions. Despite the absence of OPN, DKO bones are still hypomineralized. The SIBLING, matrix extracellular phosphoglycoprotein with ASARM motif (MEPE) is highly overexpressed in both BSP$^{-/-}$ and DKO and may impair mineralization through liberation of its ASARM (Acidic Serine-Aspartate Rich MEPE associated) peptides. DKO mice also display evidence of active formation of trabecular, secondary bone as well as primary bone in the marrow-ablation repair model. A higher number of osteoclasts form in DKO marrow cultures, with higher resorption activity, and DKO long bones display a localized and conspicuous cortical macroporosity. High bone formation and resorption parameters, and high cortical porosity in DKO mice suggest an active bone modeling/remodeling, in the absence of two key regulators of bone cell performance. This first double KO of SIBLING proteins thus results in a singular, non-trivial phenotype leading to reconsider the interpretation of each single KO, concerning in particular matrix mineralization and the regulation of bone cell activity.

1. Introduction

The SIBLING (Small Integrin-Binding LIgand, N-linked Glycoproteins) family [1] is a structurally and phylogenetically homogeneous group of skeletal tissue matrix proteins including dentin sialophosphoprotein (DSPP), dentin matrix protein-1 (DMP1), matrix extracellular phosphoglycoprotein with ASARM motif (MEPE), osteopontin/secreted phosphoprotein-1 (OPN/SPP1) and bone sialoprotein/integrin-binding sialoprotein (BSP/IBSP). Their genes are aligned in the "bone gene cluster" on human chromosome 4 (mouse chromosome 5) [2,3]. Interacting with both mineralized matrix and bone cells, SIBLING proteins are in a key position to regulate matrix properties, cell-matrix interactions as well as the dynamic response of the bone organ to environmental challenges [1]. In bone, DMP1 and MEPE are expressed mainly by osteocytes and regulate matrix mineralization and phosphate metabolism [4–6]. DSPP is mostly expressed in teeth [7] and absent in toothless vertebrate lineages [8]. BSP (review in [9]) and OPN (review in [10,11]) are highly expressed by osteoblasts, hypertrophic chondrocytes and osteoclasts. OPN is a ubiquitous factor, implicated in many physiological processes such as lactation and pathologies including inflammation, vascular calcifications and cancer; it has been described as a cytokine [12]. BSP is most intensely expressed by osteoblasts in sites of primary bone formation [13]. We previously characterized the bone phenotype of mice with a knockout (KO) of the *Ibsp* gene (BSP$^{-/-}$, [14]). Mature, 4 month old BSP$^{-/-}$ mice display low bone formation and low bone resorbing activity, but respond to tail

* Corresponding author at: LBTO, INSERM U1059, Université de Lyon - Université Jean Monnet, Pole Santé Nord - Faculté de Médecine, Rm 118, 10 Chemin de la Marandière, F 42270 St Priest en Jarez, France.
E-mail address: luc.malaval@univ-st-etienne.fr (L. Malaval).

https://doi.org/10.1016/j.bone.2018.12.001
Received 19 October 2018; Received in revised form 29 November 2018; Accepted 3 December 2018
Available online 05 December 2018
8756-3282/

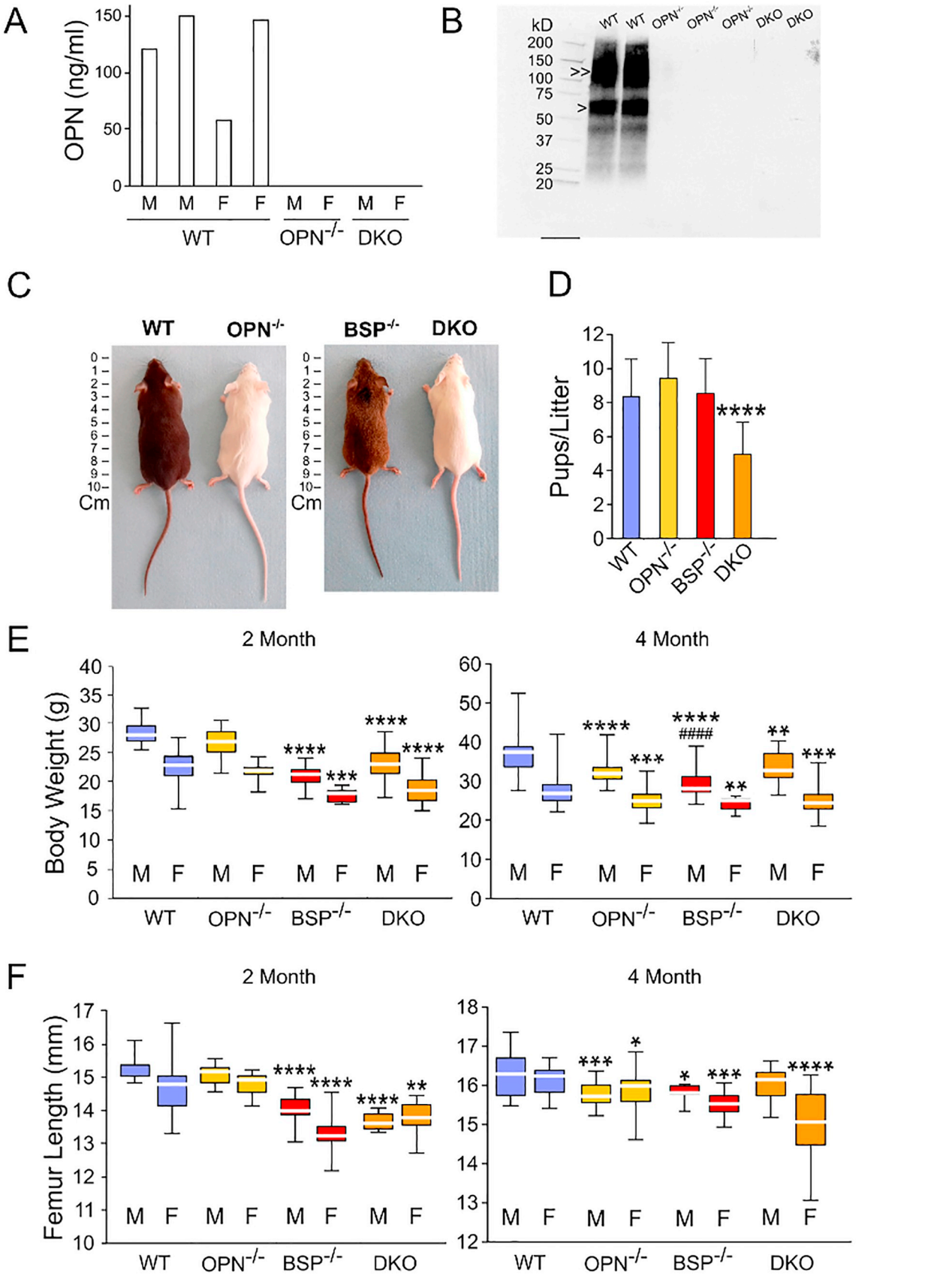

(caption on next page)

Fig. 1. Characterization of DKO mice. A: ELISA of OPN in WT and mutant serum. No protein was detected in samples from $OPN^{-/-}$ or DKO mutant mice. B: Western blotting of long bone shaft proteins extracts. OPN, both monomeric (arrowhead) and cross-linked by enzymatic activity [40] (double arrowhead) is absent from $OPN^{-/-}$ and DKO bone extracts. C: Pictures and body length of WT, $OPN^{-/-}$, $BSP^{-/-}$ and DKO, 4 month old male mice. Pelt color variability reflects the outbred character of the 129_{sv}/CD1 genetic background. D: Average number of pups in litters from all 4 genotypes. Mean ± SD of 20–27 independent reproductions. ****: $p < 0.0001$ vs WT, Student's *t*-test. Body weight (E) and femur length (F) of 2 and 4 month old male (M) and female (F) WT, $OPN^{-/-}$, $BSP^{-/-}$ and DKO mice. *: $p < 0.05$, **: $p < 0.01$, ***: $p < 0.001$, ****: $p < 0.0001$ vs sex matched WT; $^{\#\#\#\#}$: $p < 0.0001$ vs sex matched DKO; Mann-Whitney *U* test; $N = 10–57$ (weight), or 6–32 mice/group (femur length).

suspension and ovariectomy like the wild type (WT), by an increased bone turnover resulting in bone loss [9]. $OPN^{-/-}$ mice do not lose bone under either challenge [15,16]. Also $BSP^{-/-}$ bone is hypomineralized respective to WT, while the $OPN^{-/-}$ were reported to be hypermineralized [17]. BSP and OPN thus appear as key regulators of bone formation, mineralization and turnover, coexpressed in various cell types with distinct sets of functions. We recently showed that in a model of local delivery of parathyroid hormone on the calvaria bone, the expression of either BSP or OPN is required for the induction of bone accrual [18], suggesting at least partial functional substitution/compensation. Strikingly $BSP^{-/-}$ mice overexpress OPN throughout their life [19,20], indicating that their phenotype, in particular the low mineral density could reflect excessive amounts of the cognate protein. Because the question of complementarity and redundancy between these two factors has become central to their functional study, we used the TALE (Transcription activator-like effector) nuclease approach to generate in $BSP^{-/-}$ mice a knockout of the *Spp1* gene coding for OPN. We show that the singular phenotype of double KO (DKO) mice is not predictable from the features of each single KO, and highlights the importance and complexity of inter-SIBLING protein interactions in the regulation of bone biology.

2. Materials and methods

2.1. Generation and validation of TALEN engineered mouse lines

Because the *Ibsp* and *Spp1* gene are aligned on mouse chromosome 5 [2,3] we used a targeted mutation approach in $BSP^{-/-}$ mice previously generated through homologous recombination [14]. We designed two pairs of TALE nuclease subunits (TALEN) targeting *Spp1* exon 5 (Fig. S1A, Tables S1, S2), and checked that after transfection of the TALEN expression plasmids in mouse MEF cells, they were able to generate targeted mutations in *Spp1* exon 5 by the T7E1 assay (not shown). In the Plateau de Biologie Expérimentale de la Souris (PBES, ENS, Lyon, France) wild-type CD1 oocytes were fertilized in vitro with sperm taken from $BSP^{-/-}$ male mice. The eggs were microinjected with the TALEN subunits mRNAs, then implanted in pseudo-pregnant females (Fig. S1B). Mice from the first (G1) and subsequent generations were screened for *Spp1* gene mutations by PCR amplification (specific primer sequence in Table S2) and sequencing (Eurofins Genomics, Ebersberg, Germany) of the target site in DNA from clipped tail samples. Knockout of the *Ibsp* gene was assessed through RT-PCR of the same samples with specific primers as described in Fig. S2. G1 mice were crossed with wild type 129_{sv}/CD1 mice and the descent interbred in order to obtain homozygous single OPN knockout ($BSP^{+/+}$ $OPN^{-/-}$) and double BSP and OPN knockout mice ($BSP^{-/-}$ $OPN^{-/-}$, DKO). The latter were further screened for OPN mRNA and protein expression (see below). Two mouse lines were selected for the experimental work (Table S1), respectively presenting deletions of a CT dinucleotide in 2567–2568 of the reference *Spp1* gene sequence (mutation (mut)1, $OPN^{-/-}$) and of 17 nucleotides in positions 2560–2576 (mut15, DKO, Fig. S3). Both mutations disrupt the *Spp1* gene open reading frame and lead to premature termination of translation.

2.2. Care for animals and experimental procedures

For line maintenance and experimentation, the animals were housed (4 adults/cage) and bred in the PLEXAN facility (Platform for Experiments and Analysis, Faculty of Medicine, University of Saint-Etienne, Saint-Etienne, France). The procedures for the care and killing of the animals were in accordance with the European Community Standards on the care and use of laboratory animals (Ministère de l'Agriculture, France, Authorization 04827). All animal experiments were approved by the local ethical committee (Comité d'Ethique en Expérimentation Animale de la Loire CEEAL-UJM, agreement n° 98) and the Animal Welfare Committee of the PLEXAN. Mice were kept at standard temperature (23 ± 2 °C), in a light controlled environment (12 h light/12 h dark cycle). Animals were fed a standard pellet diet (SAFE_A03, Safe, Augy, France) and were allowed water ad libitum. Marrow ablation of 2 month old male mice was performed as described [25]. After analgesia by administration of buprenorphine hydrochloride (Buprecare™, Axience, France), the mice were anesthetized by intraperitoneal injection of a mixture of ketamine (50 mg/kg) and xylazine (10 mg/kg). Hair over the left knee joint was shaved, and the shaved area was cleaned with ethanol. A 0.5 cm long longitudinal skin incision was made across the knee joint and then a pre-hole was drilled in the intercondylar region of the femur with a Dremel model 395 electric drill (Dremel Multipro, Breda, the Netherlands). The content of the bone marrow was removed with Nr 20 dental files (SIMFRA, Paris, France), and the bone marrow cavity was back-flushed by injecting 5 ml of sterile PBS into the femur using a syringe attached to a 27-gauge needle. The skin incision was closed with surgical pediatric wire and cleaned with povidone-iodine (Betadine™, Meda Manufacturing, Mérignac, France). Operated mice were killed by cervical dislocation 8 days after surgery, and the ablated femur harvested and processed for microtomography and histology (see below).

2.3. Protein extraction and Western-blotting

Collected femora from 2-month-old mice were cleaned from connective tissue and cut under the metaphysis and at the proximal end of the diaphysis to isolate the shaft. Femur shafts were flushed with sterile PBS. Cortical bone samples were crushed in liquid nitrogen with a mixer mill (Sartorius, Göttingen, Germany) using steel balls. The bone powder was first washed for 3 h in 2 M NaCl, 20 mM Tris, pH 7.4 (~2.5 ml/100 mg powder), then the proteins were extracted for 3 days in 0,5 M EDTA with the same buffer and weight/volume ratio. Both steps were run with protease inhibitors (P2714, Sigma), at 4 °C under gentle vortexing. The protein extract was collected by centrifugation, filtered (40 µm), desalted on PD10 columns in 50 mM ammonium bicarbonate and freeze-dried. After rehydration in pure water, the extract was re-precipitated with the Plus One SDS-Page Clean-Up kit (GE-Healthcare Europe GmbH, Freiburg, Germany), then solubilized in Laemmli buffer. 20 µg of bone protein extracts in buffer with Dithiothreitol (50 mM) were loaded on 4–20% Mini-Protean TGX™ Precast Gels, 10 well, 30 µl (Bio-Rad Laboratories, Hercules, CA, USA) and electrophoresed at 200 V. Separated proteins were analyzed by Western blotting according to standard protocols. Briefly, proteins were transferred to nitrocellulose membranes using a fast electroblotting system (iBlot^R Dry Blotting System, Life Technologies Ltd). Membranes were probed 1 h at room temperature with mouse anti-OPN monoclonal antibody AKm2A1 (sc-21742, Santa Cruz, Dallas, Tex, USA) diluted 1:600. Membranes were washed then incubated 1 h at room temperature with horseradish peroxidase (HRP)-conjugated goat anti-mouse

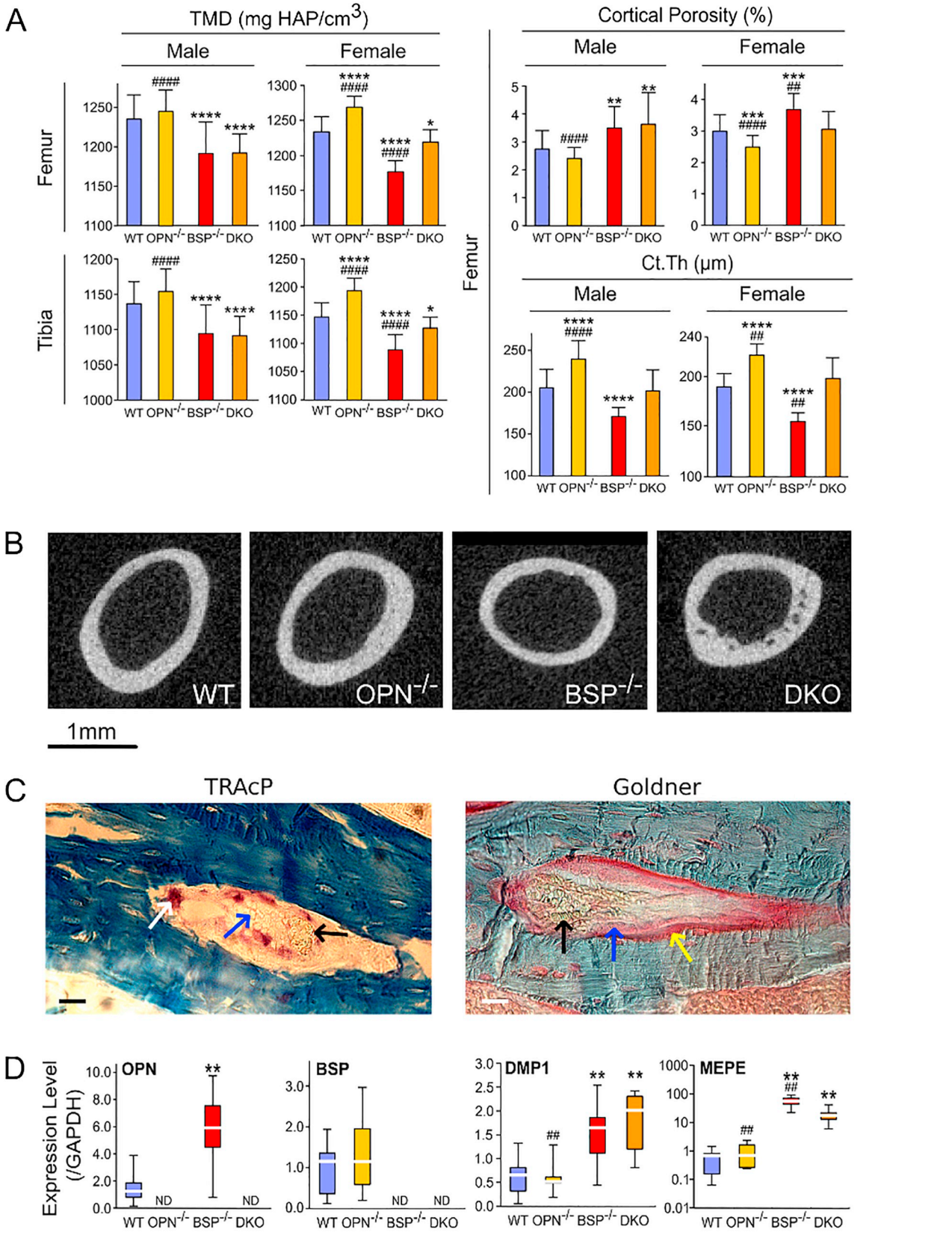

(caption on next page)

Fig. 2. Cortical bone and mineralization. A: TMD of cortical bone in femora and tibiae, Cortical Porosity and Ct.Th of femora, in 2 month old male and female mice. *: $p < 0.05$, ***: $p < 0.001$, ****: $p < 0.0001$ vs sex-matched WT; $^{\#\#}$: $p < 0.01$, $^{\#\#\#\#}$: $p < 0.0001$vs sex-matched DKO; Fisher's *t*-test or (porosity and Ct.Th at 2 month) Mann-Whitney *U* test; $N = 10–41$ mice/group. B: 2D images of the cortical bone shaft of male 2 month old femora of all 4 genotypes, showing the thinner $BSP^{-/-}$ cortex and the conspicuous porosity of the DKO. C: TRAcP histoenzymology (left) and Goldner trichrome staining (right) of undecalcified cortical femur bone of 2 month old DKO mice. White arrow: TRAcP stained osteoclast; blue arrows: cuboidal osteoblasts; black arrows: blood cells; yellow arrow: osteoid layer; Bars = 50 μm. See also Fig. S4. D: qRT-PCR of SIBLING proteins in the femoral cortical bone of 2 month old male mice. Expression is given as ratios to GAPDH. Primer sequences and meaning of abbreviations are given in Table S2. Note the log scale for MEPE. ND = Not detectable. **: $p < 0.01$ vs WT; $^{\#\#}$: $p < 0.01$ vs DKO; Mann-Whitney *U* test; $N = 6–11$ mice/group. (For interpretation of the references to color in this figure legend, the reader is referred to the web version of this article.)

secondary antibody diluted 1:8000 (Jackson ImmunoResearch Europe Ltd., Suffolk, UK), and imaging was performed with enhanced chemiluminescence detection system (Chemismart System, Vilber Lourmat, Marne-la-Vallée, France).

2.4. Blood collection and assays

Blood was collected from 2- and 4-month-old mice in Microtainer tubes (Becton Dickinson, Le Pont-de-Claix, France). The serum was separated from the clot and stored at −80 °C. Serum calcium and phosphorus were measured photometrically on a c701/Cobas 8000 Roche/Hitachi autoanalyzer (Roche Diagnostics, Switzerland) in the Medical Biology Technical Facility (Pôle de Biologie Médicale), University Hospital, Saint-Etienne. ELISA of serum OPN was performed with the DuoSet mouse Osteopontin ELISA Development System (R&D Systems, Minneapolis, MN, USA) according to the manufacturer's instructions.

2.5. Microtomography

Scans of the femora, intact or after marrow ablation, tibiae and vertebrae were acquired ex vivo after dissection, using a Viva CT40 μCT (Scanco Medical, Bassersdorf, Switzerland), at 55 keV for intact bone and 45 keV for ablated femora, with a 10 μm isotropic cubic resolution. Three-dimensional reconstructions were generated using the following parameters: σ = 1.2; support = 2; threshold = 245 for trabecular bone, 280 for cortical bone and 325 for ablated bone. The structural parameters of trabecular bone, bone volume (BV)/trabecular volume (TV), trabecular thickness (Tb.Th), trabecular number (Tb.N), trabecular separation (Tb.Sp), structure model index (SMI), and connectivity density (Conn.D) were generated from a set of 150 (femur), 160 (tibia) or 165 sections (ablated femora) under the growth plate of long bones, and between the two growth plates of the second lumbar vertebra (L2), without assuming a constant model. Cortical thickness (Ct.Th, μm), area (Ct.Ar, mm^2), porosity (=1 − (BV/TV), %) and tissue mineral density (TMD, mg of hydroxyapatite (HAP)/cm^3), as calibrated with an HAP phantom, were calculated by integration of the value on each transverse section of a set of 60 chosen in the midshaft area. The ROI for medullary bone in ablated femora was fitted to the ablated volume (Fig. 6A). Transparency imaging (Fig. S4) was performed with Protocol 2 of the Scanco vivaCT40 system, with the following parameters: σ = 1, Support = 1, lower threshold = 300, upper threshold = 500.

2.6. Histology and histomorphometry

Excised femur bones were fixed in 3.7% paraformaldehyde in PBS, dehydrated in acetone, and embedded in methylmethacrylate. Longitudinal sections were cut with a Jung model K microtome (Carl Zeiss, Heidelberg, Germany) and used for modified Goldner staining or tartrate-resistant acid phosphatase labeling of the osteoclasts. Goldner-stained sections were used to image intact or marrow ablated bone histology and for the measurement of structural parameters of trabecular bone, in particular BV/TV and Tb.Th to normalize the measurements of dynamic bone parameters. Bone formation parameters were measured after double tetracycline labeling, on unstained sections for labeled surfaces (mineralizing surface (MS)/BS, %), mineral apposition rate (MAR, μm/day), and bone formation rate (BFR)/BS (%). Osteoclast parameters, osteoclast surfaces (Oc.S/BS, %) and osteoclast numbers per bone area (N.Oc/B.Ar, mm^2), were measured on tartrate-resistant acid phosphatase (TRAcP) stained sections, after counter-staining with toluidine blue.

2.7. Quantitative real-time polymerase chain reaction analysis

Femora from 2-month-old mice were collected and cleaned from connective tissue. The shafts were cut-out and flushed with sterile PBS, then crushed in liquid nitrogen as described above for protein extraction. RNA was extracted from the bone powder or from osteoclast cultures (see below) with Tri-Reagent (Sigma), then purified on columns according to the manufacturer's instructions (Rneasy Plus Mini Kit, Qiagen, Hilden, Germany). RNA amounts were assessed with the Ribogreen kit (Invitrogen, Life Technologies, Eugene, OR, USA) and their quality checked with the Experion automated electrophoresis station (Bio-Rad, Hercules, CA, USA). Messenger RNA was reverse-transcribed (iScript cDNA synthesis Kit, Biorad) according to manufacturer's instruction, then 400 ng of cDNA were amplified through qRT-PCR using the SYBR Green I dye (Lightcycler faststart DNA masterSYBR green I, Roche, Germany). Primer sequences are given in Table S2. The expression of the housekeeping gene (GAPDH) did not vary significantly at either age in either genotype.

2.8. Osteoclast culture

Flushed-out bone marrow cells were collected from hind limbs of 8 week old mice, washed through a 100 μm pore cell strainer and loaded on a gradient of Leukocyte Separation Medium, at 1250 g for 20 min and 20 °C. Progenitor cells were recovered by aspiration of the gradient interface, washed by centrifugation and seeded in 12-well tissue culture plates (2×10^5 cells/4 cm^2) in α-MEM medium (Invitrogen) supplemented with 10% v/v FBS (Life-Technologies, Saint Aubain, France), 1% penicillin-streptomycin (Life-Technologies), 1% L-glutamine (Sigma Aldrich, Saint-Quentin Fallavier, France), 25 ng/ml Macrophage–CSF (R&D Systems, Lille, France), 100 ng/ml receptor-activated nuclear receptor factor κB ligand (RANKL). Five day cultures were fixed (4% PFA) and stained for TRAcP activity with a leucocyte acid phosphatase kit (Sigma Aldrich). Stained multinucleated cells showing > 3 nuclei were manually counted. Mineralized matrix resorption was assessed on Apatite Collagen Complex (ACC, Corning, Avon, France). Day-4 osteoclasts were detached from plastic wells by flushing after incubation at 37 °C for 5 min in PBS, 0.25 mM EDTA. They were counted and two hundred cells of each genotype were plated/well and left to resorb for 48 h. Cells were removed by gentle shaking in 0.001% Triton buffer lysis for 1 h, then the substrate was stained with silver nitrate. Resorption pits were imaged under a light microscope and images were numerized with Epsilon perfection V750 Pro scanner (Micro Epsilon, Ortenburg, Germany), and quantified semi automatically with ImageJ software (National Institutes of Health, Bethesda, MD). Data were reported as percent of mineralized surfaces resorbed, and in $μm^2$/osteoclasts after TRAcP staining and counting of reference wells. Osteoclast cultures from all 4 genotypes were extracted with Tri-Reagent and processed form qRT-PCR of SIBLING proteins as described above.

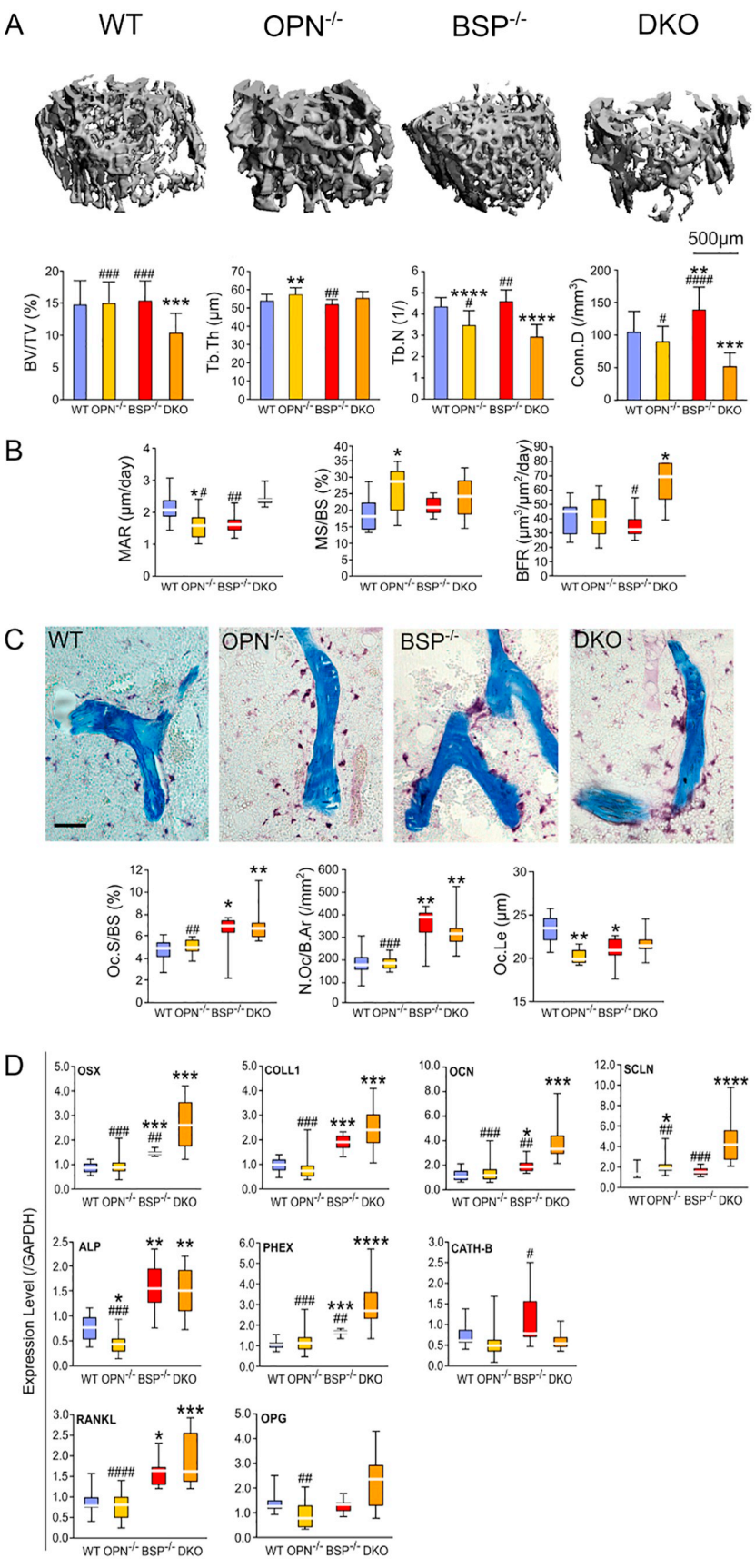

Fig. 3. Bone trabecular dynamics and osteoblast marker expression in young (2 months old) single and double KO mice. (A) Microtomographic 3D rendering, structural parameters (BV/TV, Tb.Th, Tb.N and Conn.D) and (B) cellular parameters of bone formation (MAR, MS/BS and BFR) in the trabecular bone of 2 month old WT, OPN$^{-/-}$, BSP$^{-/-}$ and DKO male mice. *: $p < 0.05$, **: $p < 0.01$, ***: $p < 0.001$, ****: $p < 0.0001$ vs age-matched WT; $^{\#\#}$: $p < 0.01$, $^{\#\#\#}$: $p < 0.001$ vs age-matched DKO; Fisher's *t*-test or (cellular parameters) Mann-Whitney *U* test; $N = 5$–34 mice/group. See also Tables S4, S5. C: Pictures of TRAcP staining and osteoclast cellular parameters (Oc.S/BS, N.Oc/B.Ar and Oc.Le) at 2 month in male mice. $N = 5$–8 mice/group. Bar = 50 µm. D: RNA expression of osteoblast markers in the femoral cortical bone of 2 month old male mice, given as ratios to GAPDH. Primer sequences and meaning of the abbreviations are given in Table S2. *: $p < 0.05$, **: $p < 0.01$, ***: $p < 0.001$, ****: $p < 0.0001$ vs WT; $^{\#\#}$: $p < 0.01$ vs DKO; Mann-Whitney *U* test; $N = 6$ to 11 mice/group.

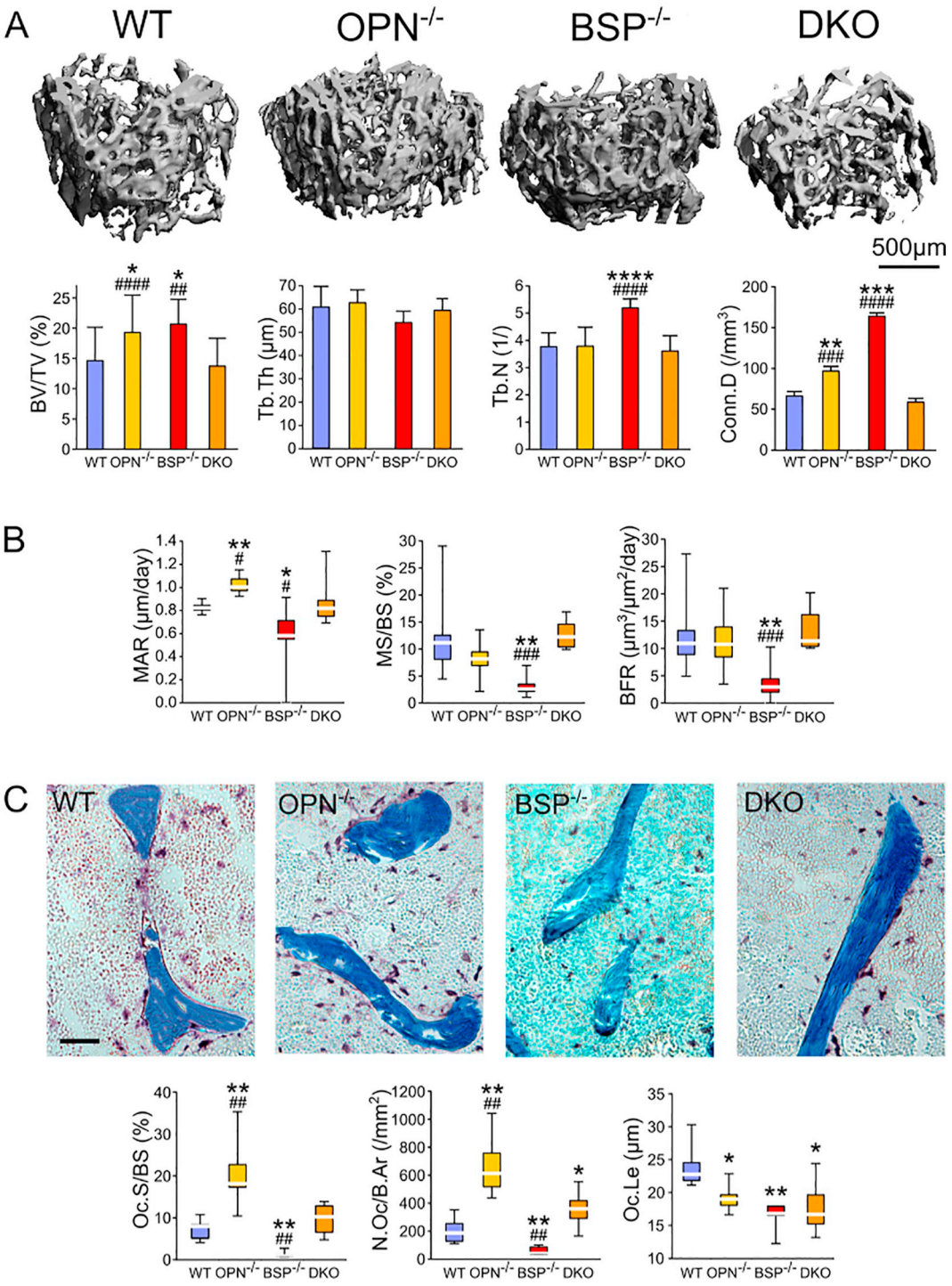

Fig. 4. Bone trabecular dynamics of mature (4 months old) single and double KO mice. (A) Microtomographic 3D rendering, structural parameters (BV/TV, Tb.Th, Tb.N and Conn.D) and (B) cellular parameters of bone formation (MAR, MS/BS and BFR) in the trabecular bone of 4 month old WT, $OPN^{-/-}$, $BSP^{-/-}$ and DKO male mice. *: $p < 0.05$, **: $p < 0.01$, ***: $p < 0.001$, ****: $p < 0.0001$ vs age-matched WT; $^{\#\#}$: $p < 0.01$, $^{\#\#\#}$: $p < 0.001$ vs age-matched DKO; Fisher's *t*-test or (cellular parameters) Mann-Whitney *U* test; $N = 5$–34 mice/group. See also Tables S4, S5. C: Pictures of TRAcP staining and osteoclast cellular parameters (Oc.S/BS, N.Oc/B.Ar and Oc.Le) at 4 month in male mice. $N = 5$–8 mice/group. Bar = 50 µm.

2.9. Statistical analysis and data presentation

Data analysis was performed with the STATISTICA software (version 8.2; StataCorp, College Station, TX). All data were tested for normal distribution (Kolmogorov–Smirnov's test) and equality of variances (Shapiro's test). Experiments for which sample size (N) was > 10 for most groups and data were found compliant were assessed with Fisher's *t*-test (litter size, microtomography), except when stated otherwise for some non-compliant samples. They are presented as average ± SD in the figures (bar charts) and tables. Parameters failing either or both requirements, or for which N was mostly < 10 (morphometry, histomorphometry), are presented as box-plots, in which the bottom and top box limits mark the first and third quartile, respectively, the horizontal line gives the median and the whiskers the range of the

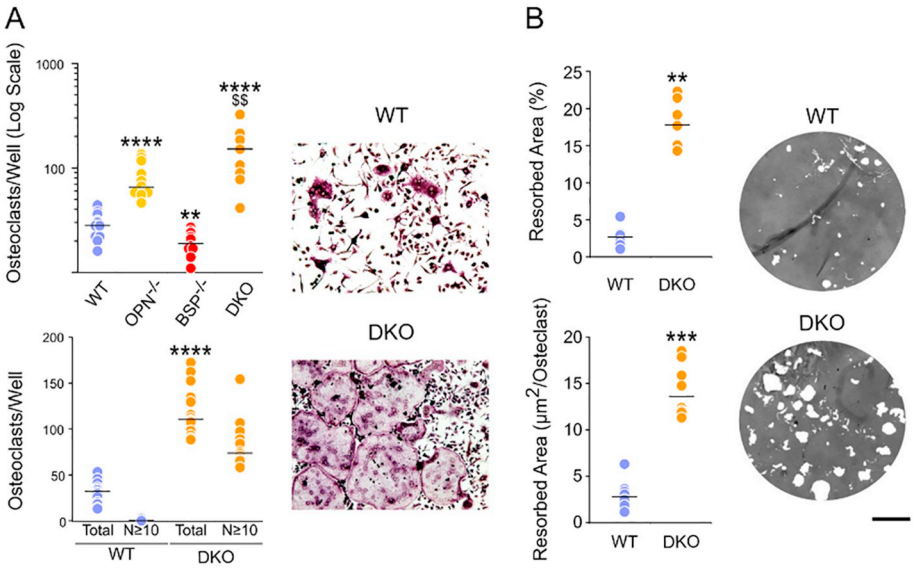

Fig. 5. In vitro osteoclast differentiation and activity. A: Quantification (left) of osteoclast differentiation in bone marrow cultures of WT, OPN$^{-/-}$, BSP$^{-/-}$ and DKO mice, and imaging (right) of WT and DKO osteoclasts. Note the log scale for osteoclast numbers on top left. B: Quantification (left) and imaging (right) of the resorption activity of replated WT and DKO osteoclasts. Osteoclast cultures were stained with hematoxylin-eosin, and the Osteologic™ disks with Von-Kossa (VK). Bar = 200 µm. *: $p < 0.05$, **: $p < 0.01$, ***: $p < 0.001$, ****: $p < 0.0001$ vs WT; $^{\#}$: $p < 0.05$, $^{\#\#}$: $p < 0.01$, $^{\#\#\#}$: $p < 0.001$ vs DKO; $^{\$\$}$: $p < 0.01$ vs OPN$^{-/-}$; Mann-Whitney *U* test. See Materials and methods for details.

data set. Results of in vitro assays are displayed as individual replicate values, with median bar. All were assessed with the non-parametric Mann–Whitney *U* test. N values are given in the figure legends.

3. Results

3.1. Generation and validation of the *Ibsp*$^{-/-}$ *Spp1*$^{-/-}$ mouse line

Forty eight percent (10/21) of *Ibsp*$^{+/-}$ offspring from eggs microinjected with TALEN mRNA (G1, Fig. S1, see Materials and methods) carried mutations in the *Spp1* gene. Several mutations were often present in the progeny of the same mouse (19 mutations generated from 10 G1 mice, Table S1), reflecting continuous activity of TALEN nucleases in the embryo after the first cell division. We crossed the founders with wild-type mice and obtained *Spp1*$^{+/mut}$ *Ibsp*$^{+/-}$ G2 offsprings, founder mice carrying the OPN and BSP mutations on the same chromosome, which were interbred to obtain double homozygous mice. G2 *Spp1*$^{+/mut}$ *Ibsp*$^{+/+}$ mice, in which the mutated *Spp1* was proximal to a wild type *Ibsp* allele were interbred to obtain simple KO of OPN in the same 129$_{sv}$/CD1 genetic background (Fig. S1). While most *Spp1* mutations did not block mRNA translation (Table S1) we identified homozygous strains (*Ibsp*$^{+/+}$ *Spp1*$^{-/-}$ and *Ibsp*$^{-/-}$ *Spp1*$^{-/-}$) in which OPN expression was fully abolished, as shown by qRT-PCR amplification spanning exons 2–3 and 2–7 (Fig. S1C), ELISA of circulating OPN protein (Fig. 1A) and Western blotting of OPN in protein extracts of femur bone shafts (Fig. 1B). One DKO line (mut15) and one OPN$^{-/-}$ line (mut1) were used for the experimental work (Table S1, DNA sequences in Fig. S3). DKO mice reach adulthood, display normal morphology (Fig. 1C) and are fertile although with smaller litter size than WT or single KO mice (Fig. 1D). Both DKO sexes are smaller (Fig. 1C) and lighter than WT at 2 and 4 months, similar to BSP$^{-/-}$ [14] and to 4 month old OPN$^{-/-}$ (Fig. 1E), with concomitantly shorter femur length (except for male DKO, Fig. 1F).

3.2. DKO long bone shaft displays bone matrix hypomineralization, conspicuous intracortical remodeling and high expression of DMP1 and MEPE

The double KO does not affect serum calcium and phosphorus levels which never differ from WT (Table S3). While remaining within normal range [21], calcium is slightly higher than WT in the BSP$^{-/-}$ at two months and lower at 4 months as reported [22] and phosphorus is significantly higher in 2 month old females. OPN$^{-/-}$ mice show higher phosphorous levels at 4 months (Table S3).

Similar to BSP$^{-/-}$, µCT of DKO mice displays lower Tissue Mineral Density (TMD) in both femur and tibia at 2 (Fig. 2A) and 4 months of age in both sexes (Tables S4, S5). While in the OPN$^{-/-}$ the cortical bone shows constantly higher TMD values than other genotypes, this is statistically significant only in young females (Fig. 2A, Table S5). Cortical thickness (Ct.Th) and area (Ct.Ar) of DKO femora do not differ from WT, while the Ct.Ar of the tibiae is higher at 4 months (Tables S4, S5). In single KO mice, OPN$^{-/-}$ cortical bone is thicker than WT at 2 months (with higher Ct.Ar in both long bones, Fig. 2A, Tables S4, S5), while the Ct.Th of BSP$^{-/-}$ femora is constantly lower than WT as previously shown (Fig. 2A, Table S5, [14]), and the Ct.Ar is higher in adult female tibiae (Tables S4, S5). Male DKO and BSP$^{-/-}$ mice display higher cortical porosity than WT, as measured in µCT, in femora (Fig. 2A) and in tibiae at 2 months (Table S4). Cortical porosity of female DKO is higher than WT only in 4 month old tibiae (Table S5).

While the bone structure of BSP$^{-/-}$ femoral cortices looks homogeneous, DKO femora display striking macroporosity (Figs. 2B, S4). Intracortical cavities are located in the posterior side of the midshaft (Figs. 2B, S4B) in connection with the marrow space (Fig. S4B). They are less developed in females (Fig. S4C) and also observed in tibiae (Fig. S4D). These spaces contain blood vessels along with a lining of osteoid-laying osteoblasts, and labelling for tartrate resistant acid phosphatase (TRAcP) also shows abundant osteoclasts (Fig. 2C), all signs of active remodeling.

Quantitative RT-PCR analysis of SIBLING gene expression in the flushed femoral bone shaft of all 4 genotypes (Fig. 2D) confirms the extinction of target proteins in mutant lines and the overexpression of OPN in BSP$^{-/-}$ bone previously reported [19]. Two other SIBLING proteins are found overexpressed in DKO and BSP$^{-/-}$, DMP1 (~2 and ~1.5 fold, respectively vs WT) and most strikingly MEPE. RNA expression for MEPE is 33 fold higher in DKO than in WT (respective medians: 17.4 vs 0.7, $N = 7$, $p < 0.01$, Mann-Whitney *U* test), and ~80 fold in the BSP$^{-/-}$ (median: 56.4, $p < 0.01$, Fig. 2D).

3.3. Young DKO mice present with high trabecular bone activity

Single and double KO of BSP and OPN affect the dynamics of trabecular bone. In young (2 month old) mice, µCT analysis shows lower trabecular bone volume (BV/TV) in male DKO femur (Fig. 3A). This goes with reduced trabecular number (Tb.N) and connection density (Conn.D, Fig. 3A) and converse higher trabecular separation (Tb.Sp, Table S4). While femur BV/TV does not differ from WT in young single

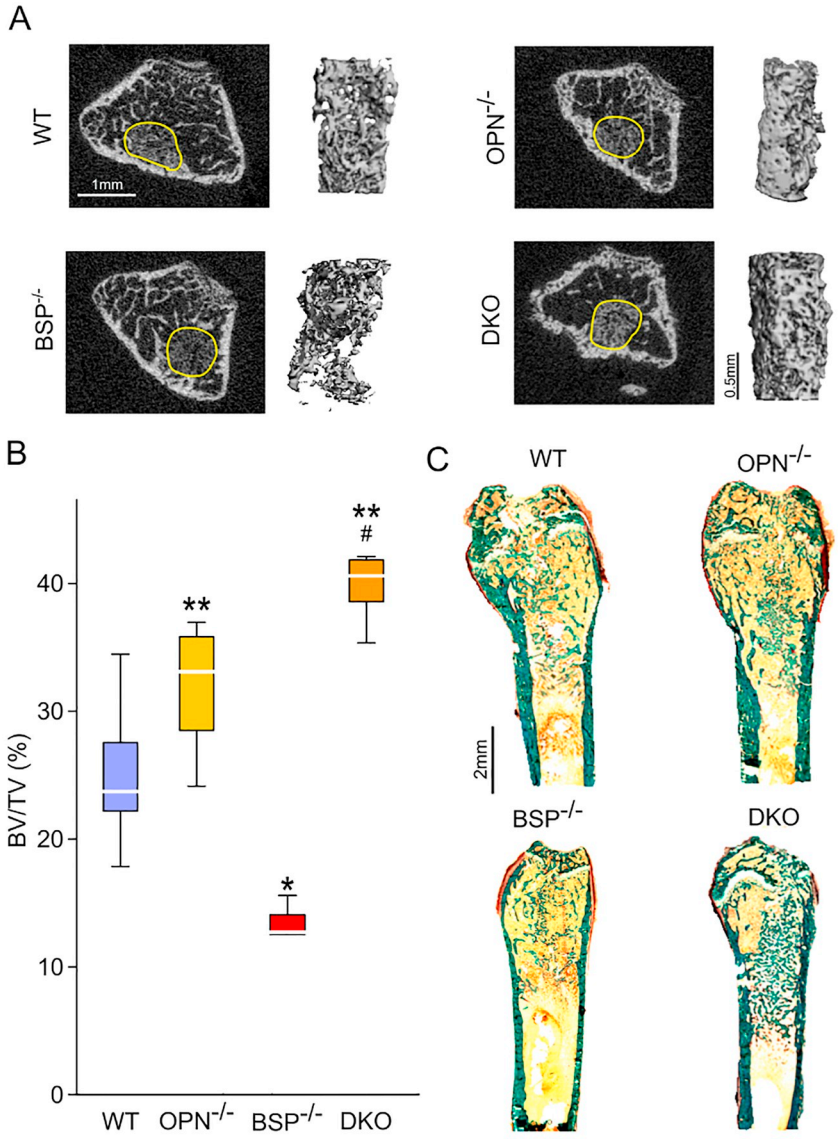

Fig. 6. Medullary bone formation after marrow ablation. A: 2D μCT images (metaphysis section) and 3D reconstruction, B: quantification, C: Goldner's trichrome staining of medullary bone formed 8 days after marrow ablation in the femur of 2 month old WT, OPN$^{-/-}$, BSP$^{-/-}$ and DKO male mice. In A the ROI for quantification is outlined in yellow. *: $p < 0.05$, **: $p < 0.01$ vs WT; $^{\#}$: $p < 0.05$ vs DKO; Mann-Whitney U test; $N = 6$ mice/group except for BSP$^{-/-}$, $N = 3$. See Materials and methods for details. (For interpretation of the references to color in this figure legend, the reader is referred to the web version of this article.)

KO male mice, trabeculae are thicker and less numerous in the OPN$^{-/-}$, while they are more connected and tend to be thinner and more numerous in the BSP$^{-/-}$ (Fig. 3A). A similar profile is observed in tibiae (Table S4). Histomorphometry reveals a high cellular activity in young DKO trabecular bone, with higher bone formation (Mineral Apposition Rate, MAR, and Bone Formation Rate, BFR) while the OPN$^{-/-}$ and BSP$^{-/-}$ have a similar BFR level as the WT at this age, with lower MAR but higher Mineralizing Surfaces (MS/BS) for the OPN$^{-/-}$ (Fig. 3B). Surfaces (Oc.S/BS) and numbers (N.Oc/B.Ar, Fig. 3C) of the resorbing cells osteoclasts are higher than WT in young DKO mice, along with the BSP$^{-/-}$, but with shorter osteoclast length (Oc.Le) in mutant bones (Fig. 3C).

High cellular activity in 2 month old DKO mice is reflected in mRNA expression levels assessed in cortical bone (Fig. 3D). Early osteoblast differentiation markers OSX, COLL1 and ALP, as well as the mature marker of osteoblast maturity OCN, the mature osteocyte marker SCLN and membrane protein PHEX, and the pro-resorbing cytokine RANKL are all overexpressed in DKO bones (Fig. 3D). This is also observed, often to a lesser extent, in the BSP$^{-/-}$.

In mature, 4 months old male DKO femur trabecular BV/TV no longer differs from the WT, while it is higher in the OPN$^{-/-}$ and, as reported [14], in the BSP$^{-/-}$ (Fig. 4A). Mature BSP$^{-/-}$ femur displays more numerous trabeculae, and both single KO present with higher connection density (Fig. 4A). The same is observed in male tibiae at this age (Table S4). Formation parameters measured in femur of mature mice mark a lower overall activity, with similar values to WT for mature DKO, while the OPN$^{-/-}$ display higher MAR, and the BSP$^{-/-}$ show markedly reduced MS/BS, MAR and BFR, as previously described (Fig. 4B, [14,22]). N.Oc/B.Ar remain high in 4 months old DKO while the OC·S/BS no longer differ from WT, and Oc.Le is lower (Fig. 4C). Oc.S/BS and N.Oc/B.Ar are found increased in mature OPN$^{-/-}$ (Fig. 4C), while they are very low in mature BSP$^{-/-}$ as previously reported [14,22].

The dynamic of the trabecular compartment in male vertebrae differs from appendicular bones, with the same BV/TV as WT in all young mutant mice and significantly higher values in all mature KO (Table S4). The bone phenotypes of mutant female mice is more contrasted, with higher BV/TV in the OPN$^{-/-}$ at all sites and ages, and time- and

Table 1
SIBLING gene expression and bone matrix mineralization in gene-targeted mouse models.

Reference	SIBLING protein expression (~x WT)				Mineralization	Remark
	BSP	OPN	DMP1	MEPE		
	x1	KO	x1	x1	≃/↑	
This study	KO	**x2**	**x3**	**x80**	↓	
	KO	KO	**x2.5**	**x33**	↓	
6	**x10**	**x10**	KO	**x5**	↓	High FGF23, rickets
5	?	**x2**	x1	KO	≃	
35	?	x1–**x0.5***	**x3**	**x10**	↓	MEPE Tgn, cf discussion
29	?	**x3***	?	?	↓	ALP$^{-/-}$
30	?	**x2**	?	?	↓	FGF23$^{-/-}$

SIBLING expression as assessed by qRT-PCR of bone mRNA (except for *: Western-blot on bone extract) and given as approximative multiple (~x, in bold when ≠ 1) of WT levels. KO: Gene knockout. Tgn: Transgenic. "↑": Increased, "↓": Decreased, "~/↑": Age and/or sex variable phenotype, "≃": Same, all vs WT. "?": Information missing. Yellow backgrounds mark the targets of genetic alteration in the mouse models. Data from the papers given in Reference, see Bibliography.

skeletal site-variable values for DKO and BSP$^{-/-}$ (Table S5).

3.4. Deletion of both OPN and BSP results in higher osteoclast differentiation and activity in vitro

Much more osteoclast cells differentiated in bone marrow cultures from DKO mice than the WT, and they were bigger, with more nuclei (Fig. 5A). Osteoclasts were also more numerous in OPN$^{-/-}$ cultures and were in contrast scantier in the BSP$^{-/-}$, as published [23,24]. In vitro DKO osteoclasts resorbed a ~7 fold higher area of mineralized substrates than WT ones, in total and on a per cell basis (Fig. 5B). Quantitative RT-PCR screening of WT and mutant osteoclast cultures did not detect the expression of any other SIBLING family member than BSP and OPN (not shown).

3.5. DKO mice respond to marrow ablation with enhanced medullary bone formation

Marrow ablation of rodent bones launches a cycle of rapid (~8 days) building of primary bone inside the ablated volume of the shaft (medullary bone, Fig. 6A), which is later resorbed with return to normal bone marrow. As previously showed [25], marrow ablated BSP$^{-/-}$ mice form a (~50%) lower amount of medullary bone than WT (Fig. 6B). In contrast, we found that in this model of primary osteogenesis OPN$^{-/-}$ mice form a higher volume of primary bone 8 days after ablation (Fig. 6B). Strikingly, the volume is even higher in DKO ablated mice, reaching nearly twice the amount present in the WT as shown by μCT analysis (Fig. 6A, B) and Goldner staining of undecalcified sections (Fig. 6C).

4. Discussion

Mouse KO of individual SIBLING genes [4,7,14,24,26] display quite diverse phenotypic effects, suggesting specific roles for each family member. Globally however, this family has been studied until now through a "single gene" approach and analyzing the interplay between its members now requires multiple targeting strategies. This is particularly important for the establishment and clarification of the specific functions of OPN and BSP in the bone organ and tissue. Here we used sequence-specific TALEN nucleases to knock out the *Spp1* gene in BSP$^{+/-}$ mice. We were thus able to isolate null *Spp1* alleles associated with either wild-type or null alleles of the BSP gene lying in tandem, the first double KO within this family of proteins. We then compared DKO mice with OPN$^{-/-}$, BSP$^{-/-}$ and WT lines in the same genetic background. DKO mutants are healthy, and their reduced fertility can be linked to previous works hinting at BSP [27] and OPN [28] involvement in pregnancy.

Overexpression of OPN, as observed in BSP$^{-/-}$ mice has been linked to impaired bone matrix mineralization. In high-OPN expressing ALP(Akp2)$^{-/-}$ [29] and FGF23$^{-/-}$ mutant mice ([29], Table 1) mineralization recovered partially or totally after crossing with the OPN$^{-/-}$. The converse hypermineralization of OPN$^{-/-}$ bone matrix has been

previously reported [17] and found significant in our μCT analysis only in young females (Fig. 2, Table S5). That the cortical bone of DKO mice is hypomineralized as in the BSP$^{-/-}$ suggests that high OPN does not explain the mineralization defect in the BSP knockout. While other factors may impact mineralization in the absence of BSP, such as the recently reported increased levels of pyrophosphate in BSP$^{-/-}$ plasma [31], we found that both BSP$^{-/-}$ and DKO bone over-express the other SIBLING members, DMP1 and MEPE. MEPE, whose mRNA amount is tremendously increased in BSP$^{-/-}$ and DKO shafts, is described as a major inhibitor of bone mineralization through its cleavage by CATH-B and liberation of the ASARM (Acidic Serine-Aspartate Rich MEPE associated) peptide [32–34]. Transgenic mice overexpressing MEPE under the collagen 1 (Col1α1-2.3kb) promoter (MEPE Tgn, [35]) display shorter stature, lower matrix mineralization and reduced bone formation and resorption. These features are also observed in adult BSP$^{-/-}$ mice [14,34] and except for bone cellular activity in the DKO. However, MEPE Tgn mice also present with lower ALP expression, reduced OPN protein amounts (with normal mRNA levels, Table 1) as well as hypercalcemia and hyperphosphatemia at ~4 months under normal diet. In contrast BSP$^{-/-}$ mice over-express OPN and ALP, and are normo-phosphatemic and slightly hypocalcemic at this age ([22], Table S3) and DKO blood calcium and phosphate never differ from WT. Therefore detailed analysis of MEPE expression as well as calcium and phosphate metabolism in BSP$^{-/-}$ and DKO mice will be required to unravel the mechanisms involved in their phenotypes and similarities/differences with the MEPE Tgn. Of note, the membrane endopeptidase PHEX, shown to degrade ASARM [36] and prevent its release from MEPE [37] is also overexpressed in BSP$^{-/-}$ and DKO bones (Fig. 3D). It will thus be important to establish whether the high production of ASARM peptides observed in the MEPE tgn [35] also occurs in BSP$^{-/-}$ and DKO mice and contributes to their hypomineralized phenotype. Interestingly, MEPE was found over-expressed in all SIBLING gene-targeted mouse models where bone mineralization is altered, not always along with high OPN (Table 1). As mentioned, crossing with OPN$^{-/-}$ did compensate the hypomineralized phenotype of Akp2$^{-/-}$ and FGF23$^{-/-}$ mice [29,30], but to our knowledge expression of MEPE (or DMP1, another source of ASARM peptide) has not been assessed in these double-KO lines (Table 1), and its role remains to be evaluated.

The trabecular bone phenotype of our three mutant lines presents with sex-, time- and site-specificities. Thus BSP$^{-/-}$ mice, whose long bones at 2 months (but not female vertebrae, Table S5) present with normal BV/TV, as well as normal bone forming parameters and higher molecular markers of formation and resorption, display at 4 months concomitant low cellular activity and high trabecular volume as documented in earlier studies [14,22]. We previously described the same high bone volume (with reduced osteoclast surfaces) in much younger (3 week old) BSP$^{-/-}$ mutants [20]. The present findings suggest either a more complex time-course of BSP$^{-/-}$ bone dynamics (with successive phases of low and high cellular activity) than anticipated, or a shift in phenotype of our line, whose cause is unknown but which may stem from recent modifications of housing conditions (fewer mice per cage, enriched environment). Strikingly, young (2 month old) DKO mice display lower leg bone BV/TV than WT along with higher histomorphometric and molecular markers of bone formation and resorption (Fig. 3). In mature (4 month old) DKO mice, both BV/TV and cellular activity are similar to WT, while OPN$^{-/-}$ and BSP$^{-/-}$ display higher trabecular volume at this age, at least in tibiae (Fig. 4, Tables S4, S5). Overall, DKO mice thus display a level of bone formation activity which is equal or superior to WT. This is confirmed by marrow ablation experiments in which double mutants lay higher amounts of primary bone, a feature also found in the OPN$^{-/-}$ but to a lesser extent (Fig. 6). This again contrasts with the BSP$^{-/-}$ where the amount of medullary bone is reduced (Fig. 6, [25]), and suggests that the concomitant elimination of OPN reverts the effects of the absence of BSP, in primary (medullary bone) as well as secondary bone formation (cf BFR).

A very singular feature of DKO cortical bone is its macroporosity, most conspicuous in males (Figs. 2, S4, Tables S4, S5) with strong indication of active local bone turnover. Significant number and activity of osteoclast cells in DKO mice is to be expected from the high RANKL levels in vivo as well as the higher rate of osteoclast formation, fusion and resorption activity by DKO cells in vitro. Because in vitro osteoclast differentiation and/or activity have been shown to be impaired in OPN$^{-/-}$ [24,38] and BSP$^{-/-}$ [23] mutants, this intriguing observation suggests the expression of compensating factors - but not other SIBLING family members, ruled out by our qRT-PCR results. In contrast, the lower average osteoclast length in all mutant lines suggests a still impaired cellular functionality in vivo, maybe compensated at least in DKO by higher osteoclast numbers.

Several striking differences between the bone phenotypes of BSP$^{-/-}$ and DKO mice can thus be attributed to OPN over-expression in the BSP$^{-/-}$. Normalized cortical thickness and bone formation parameters in mature DKO mice, along with increased medullary bone formation after ablation strongly suggest that inhibition of osteoprogenitor recruitment and/or osteoblast activity is induced by high OPN in BSP$^{-/-}$ long bones, as was documented in vitro for normal osteoblastic cells [39]. As discussed above, high OPN does not seem to be involved in the lower TMD of the two mutant line, for which the best candidate is the very high level of MEPE expression. While DMP1 might also be a source of ASARM, on the basis of knockout phenotypes the over-expression of DMP1 and ALP in BSP$^{-/-}$ and DKO cortical bones is expected to promote mineralization. Further SIBLING-deleted mouse models might be required to dissect the interplay between these factors.

In summary, we have generated and describe here the first double KO of SIBLING proteins, OPN and BSP. This double deletion results in a singular phenotype, not predictable from the features of single KO mice and which leads to reconsider their interpretation. Our work highlights the importance of the interplay between SIBLING proteins in the regulation of bone biology, and specifically matrix mineralization, a major determinant of bone strength.

Acknowledgements

The authors thank the teams of PBES (“Plateau de Biologie Expérimentale de la Souris”, ENS de Lyon, Lyon, France) and PLEXAN for skillful technical assistance, Dr Nadia Boutahar (Medical Biology Technical Facility, University Hospital, Saint-Etienne) for calcium/phosphorus assay, Dr Myriam Normand (U1059) for advice on statistics, Dr Maura Strigini (U1059) for comments on the manuscript, Marine Charpentier, Damien Cleret, Mélanie Dhayer, Dr Benoit Dechaumet, Alix Malaval, Quentin Presles and Fadila Saidi for technical support.

Author contributions

JPC and JBR designed, produced and validated the TALEN pairs for the transfection experiments carried out by DA and MT. WB, LJ, LVe, MT and AVB carried out mouse line production and characterization, as well as in vivo experiments. IMG and OP performed the in vitro experiments. NL, DF, CT, EG and HF contributed to validating the mutations and performing bone imaging and 3D structural analysis. LM, LVi, MHLP and HF designed the project whose progression was supervised by WB. LM wrote the paper, with contribution from all other authors. WB and LM take responsibility for the integrity of the data analysis.

Funding

The “Agence Nationale de la Recherche” (grants ANR-13-BSV1-0010-01 “Mouse_Kosto” to LM and ANR-II-INSB-00014 to JPC), the “Institut National de la Santé et de la Recherche Médicale” (INSERM), the “Université Jean-Monnet” of Saint Etienne, the “Région Auvergne-Rhône-Alpes” (PhD scholarships for WB and LJ).

Disclosure

The authors have nothing to disclose.

Appendix A. Supplementary data

Supplementary data to this article can be found online at https://doi.org/10.1016/j.bone.2018.12.001.

References

[1] L.W. Fisher, N.S. Fedarko, Six genes expressed in bones and teeth encode the current members of the SIBLING family of proteins, Connect. Tissue Res. 44 (Suppl. 1) (2003) 33–40.

[2] P.S. Rowe, P.A. de Zoysa, R. Dong, H.R. Wang, K.E. White, M.J. Econs, C.L. Oudet, MEPE, a new gene expressed in bone marrow and tumors causing osteomalacia, Genomics 67 (2000) 54–68.

[3] M. MacDougall, D. Simmons, T.T. Gu, J. Dong, MEPE/OF45, a new dentin/bone matrix protein and candidate gene for dentin diseases mapping to chromosome 4q21, Connect. Tissue Res. 43 (2002) 320–330.

[4] J.Q. Feng, L.M. Ward, S. Liu, Y. Lu, Y. Xie, B. Yuan, X. Yu, F. Rauch, S.I. Davis, S. Zhang, H. Rios, M.K. Drezner, L.D. Quarles, L.F. Bonewald, K.E. White, Loss of DMP1 causes rickets and osteomalacia and identifies a role for osteocytes in mineral metabolism, Nat. Genet. 38 (2006) 1310–1315.

[5] L.V. Zelenchuk, A.-M. Hedge, P.S.N. Rowe, Age dependent regulation of bone-mass and renal function by the MEPE ASARM-motif, Bone 79 (2015) 131–142, https://doi.org/10.1016/j.bone.2015.05.030.

[6] P.H. Jani, M.P. Gibson, C. Liu, H. Zhang, X. Wang, Y. Lu, C. Qin, Transgenic expression of Dspp partially rescued the long bone defects of Dmp1-null mice, Matrix Biol. J. Int. Soc. Matrix Biol. 52–54 (2016) 95–112, https://doi.org/10.1016/j.matbio.2015.12.001.

[7] T. Sreenath, T. Thyagarajan, B. Hall, G. Longenecker, R. D'Souza, S. Hong, J.T. Wright, M. MacDougall, J. Sauk, A.B. Kulkarni, Dentin sialophosphoprotein knockout mouse teeth display widened predentin zone and develop defective dentin mineralization similar to human dentinogenesis imperfecta type III, J. Biol. Chem. 278 (2003) 24874–24880, https://doi.org/10.1074/jbc.M303908200.

[8] D.A. McKnight, L.W. Fisher, Molecular evolution of dentin phosphoprotein among toothed and toothless animals, BMC Evol. Biol. 9 (2009) 299, https://doi.org/10.1186/1471-2148-9-299.

[9] W. Bouleftour, L. Juignet, G. Bouet, R.N. Granito, A. Vanden-Bossche, N. Laroche, J.E. Aubin, M.-H. Lafage-Proust, L. Vico, L. Malaval, The role of the SIBLING, bone sialoprotein in skeletal biology - contribution of mouse experimental genetics, Matrix Biol. J. Int. Soc. Matrix Biol. 52–54 (2016) 60–77, https://doi.org/10.1016/j.matbio.2015.12.011.

[10] J. Sodek, B. Ganss, M.D. McKee, Osteopontin, Crit. Rev. Oral Biol. Med. 11 (2000) 279–303.

[11] D.T. Denhardt, M. Noda, A.W. O'Regan, D. Pavlin, J.S. Berman, Osteopontin as a means to cope with environmental insults: regulation of inflammation, tissue remodeling, and cell survival, J. Clin. Invest. 107 (2001) 1055–1061, https://doi.org/10.1172/JCI12980.

[12] V. Subraman, M. Thiyagarajan, N. Malathi, S.T. Rajan, OPN - revisited, J. Clin. Diagn. Res. JCDR 9 (2015) ZE10–13, https://doi.org/10.7860/JCDR/2015/12872.6111.

[13] R.J. Midura, A. Wang, D. Lovitch, D. Law, K. Powell, J.P. Gorski, Bone acidic glycoprotein-75 delineates the extracellular sites of future bone sialoprotein accumulation and apatite nucleation in osteoblastic cultures, J. Biol. Chem. 279 (2004) 25464–25473.

[14] L. Malaval, N.M. Wade-Gueye, M. Boudiffa, J. Fei, R. Zirngibl, F. Chen, N. Laroche, J.P. Roux, B. Burt-Pichat, F. Duboeuf, G. Boivin, P. Jurdic, M.H. Lafage-Proust, J. Amedee, L. Vico, J. Rossant, J.E. Aubin, Bone sialoprotein plays a functional role in bone formation and osteoclastogenesis, J. Exp. Med. 205 (2008) 1145–1153.

[15] M. Ishijima, S.R. Rittling, T. Yamashita, K. Tsuji, H. Kurosawa, A. Nifuji, D.T. Denhardt, M. Noda, Enhancement of osteoclastic bone resorption and suppression of osteoblastic bone formation in response to reduced mechanical stress do not occur in the absence of osteopontin, J. Exp. Med. 193 (2001) 399–404.

[16] H. Yoshitake, S.R. Rittling, D.T. Denhardt, M. Noda, Osteopontin-deficient mice are resistant to ovariectomy-induced bone resorption, Proc. Natl. Acad. Sci. U.S.A. 96 (1999) 8156–8160.

[17] A.L. Boskey, L. Spevak, E. Paschalis, S.B. Doty, M.D. McKee, Osteopontin deficiency increases mineral content and mineral crystallinity in mouse bone, Calcif. Tissue Int. 71 (2002) 145–154.

[18] W. Bouleftour, G. Bouet, R.N. Granito, M. Thomas, M.-T. Linossier, A. Vanden-Bossche, J.E. Aubin, M.-H. Lafage-Proust, L. Vico, L. Malaval, Blocking the expression of both bone sialoprotein (BSP) and osteopontin (OPN) impairs the anabolic action of PTH in mouse calvaria bone, J. Cell. Physiol. 230 (2015) 568–577, https://doi.org/10.1002/jcp.24772.

[19] R.N. Granito, W. Bouleftour, O. Sabido, C. Lescale, M. Thomas, J.E. Aubin, M. Goodhardt, L. Vico, L. Malaval, Absence of bone sialoprotein (BSP) alters profoundly hematopoiesis and upregulates osteopontin, J. Cell. Physiol. 230 (2015) 1342–1351, https://doi.org/10.1002/jcp.24877.

[20] W. Bouleftour, M. Boudiffa, N.M. Wade-Gueye, G. Bouët, M. Cardelli, N. Laroche, A. Vanden-Bossche, M. Thomas, E. Bonnelye, J.E. Aubin, L. Vico, M.H. Lafage-Proust, L. Malaval, Skeletal development of mice lacking bone sialoprotein (BSP)–impairment of long bone growth and progressive establishment of high trabecular bone mass, PLoS One 9 (2014) e95144, , https://doi.org/10.1371/journal.pone.0095144.

[21] C. Mazzaccara, G. Labruna, G. Cito, M. Scarfò, M.D. Felice, L. Pastore, L. Sacchetti, Age-related reference intervals of the main biochemical and hematological parameters in C57BL/6J, 129SV/EV and C3H/HeJ mouse strains, PLoS One 3 (2008) e3772, , https://doi.org/10.1371/journal.pone.0003772.

[22] N.M. Wade-Gueye, M. Boudiffa, N. Laroche, A. Vanden-Bossche, C. Fournier, J.E. Aubin, L. Vico, M.H. Lafage-Proust, L. Malaval, Mice lacking bone sialoprotein (BSP) lose bone after ovariectomy and display skeletal site-specific response to intermittent PTH treatment, Endocrinology 151 (2010) 5103–5113.

[23] M. Boudiffa, N.M. Wade-Gueye, A. Guignandon, A. Vanden-Bossche, O. Sabido, J.E. Aubin, P. Jurdic, L. Vico, M.H. Lafage-Proust, L. Malaval, Bone sialoprotein deficiency impairs osteoclastogenesis and mineral resorption in vitro, J. Bone Min. Res. 25 (2010) 2393–2403.

[24] S.R. Rittling, H.N. Matsumoto, M.D. McKee, A. Nanci, X.R. An, K.E. Novick, A.J. Kowalski, M. Noda, D.T. Denhardt, Mice lacking osteopontin show normal development and bone structure but display altered osteoclast formation in vitro, J. Bone Miner. Res. Off. J. Am. Soc. Bone Miner. Res. 13 (1998) 1101–1111, https://doi.org/10.1359/jbmr.1998.13.7.1101.

[25] N.M. Wade-Gueye, M. Boudiffa, A. Vanden-Bossche, N. Laroche, J.E. Aubin, L. Vico, M.H. Lafage-Proust, L. Malaval, Absence of bone sialoprotein (BSP) impairs primary bone formation and resorption: the marrow ablation model under PTH challenge, Bone 50 (2012) 1064–1073.

[26] L.C. Gowen, D.N. Petersen, A.L. Mansolf, H. Qi, J.L. Stock, G.T. Tkalcevic, H.A. Simmons, D.T. Crawford, K.L. Chidsey-Frink, H.Z. Ke, J.D. McNeish, T.A. Brown, Targeted disruption of the osteoblast/osteocyte factor 45 gene (OF45) results in increased bone formation and bone mass, J. Biol. Chem. 278 (2003) 1998–2007, https://doi.org/10.1074/jbc.M203250200.

[27] G. Cogan, A.K. Bansal, S. Ibrahim, B. Zhu, H.A. Goldberg, B. Ganss, S. Cheifetz, F.P. Armbruster, J. Sodek, Analysis of human bone sialoprotein in normal and pathological tissues using a monoclonal antibody (BSP 1.2 mab), Connect. Tissue Res. 45 (2004) 60–71, https://doi.org/10.1080/03008200490278151.

[28] Q.-R. Qi, Q.-Z. Xie, X.-L. Liu, Y. Zhou, Osteopontin is expressed in the mouse uterus during early pregnancy and promotes mouse blastocyst attachment and invasion in vitro, PLoS One 9 (2014) e104955, , https://doi.org/10.1371/journal.pone.0104955.

[29] D. Harmey, L. Hessle, S. Narisawa, K.A. Johnson, R. Terkeltaub, J.L. Millán, Concerted regulation of inorganic pyrophosphate and osteopontin by akp2, enpp1, and ank: an integrated model of the pathogenesis of mineralization disorders, Am. J. Pathol. 164 (2004) 1199–1209, https://doi.org/10.1016/S0002-9440(10)63208-7.

[30] Q. Yuan, Y. Jiang, X. Zhao, T. Sato, M. Densmore, C. Schüler, R.G. Erben, M.D. McKee, B. Lanske, Increased osteopontin contributes to inhibition of bone mineralization in FGF23-deficient mice, J. Bone Miner. Res. Off. J. Am. Soc. Bone Miner. Res. 29 (2014) 693–704, https://doi.org/10.1002/jbmr.2079.

[31] M. Ao, M.B. Chavez, E.Y. Chu, K.C. Hemstreet, Y. Yin, M.C. Yadav, J.L. Millán, L.W. Fisher, H.A. Goldberg, M.J. Somerman, B.L. Foster, Overlapping functions of bone sialoprotein and pyrophosphate regulators in directing cementogenesis, Bone 105 (2017) 134–147, https://doi.org/10.1016/j.bone.2017.08.027.

[32] A. Martin, V. David, J.S. Laurence, P.M. Schwarz, E.M. Lafer, A.-M. Hedge, P.S.N. Rowe, Degradation of MEPE, DMP1, and release of SIBLING ASARM-peptides (minhibins): ASARM-peptide(s) are directly responsible for defective mineralization in HYP, Endocrinology 149 (2008) 1757–1772, https://doi.org/10.1210/en.2007-1205.

[33] P.S.N. Rowe, The chicken or the egg: PHEX, FGF23 and SIBLINGs unscrambled, Cell Biochem. Funct. 30 (2012) 355–375, https://doi.org/10.1002/cbf.2841.

[34] P.S. Rowe, A unified model for bone-renal mineral and energy metabolism, Curr. Opin. Pharmacol. 22 (2015) 64–71, https://doi.org/10.1016/j.coph.2015.03.006.

[35] V. David, A. Martin, A.-M. Hedge, P.S.N. Rowe, Matrix extracellular phosphoglycoprotein (MEPE) is a new bone renal hormone and vascularization modulator, Endocrinology 150 (2009) 4012–4023, https://doi.org/10.1210/en.2009-0216.

[36] W.N. Addison, Y. Nakano, T. Loisel, P. Crine, M.D. McKee, MEPE-ASARM peptides control extracellular matrix mineralization by binding to hydroxyapatite: an inhibition regulated by PHEX cleavage of ASARM, J. Bone Miner. Res. Off. J. Am. Soc. Bone Miner. Res. 23 (2008) 1638–1649, https://doi.org/10.1359/jbmr.080601.

[37] R. Guo, P.S.N. Rowe, S. Liu, L.G. Simpson, Z.-S. Xiao, L.D. Quarles, Inhibition of MEPE cleavage by Phex, Biochem. Biophys. Res. Commun. 297 (2002) 38–45.

[38] M.A. Chellaiah, N. Kizer, R. Biswas, U. Alvarez, J. Strauss-Schoenberger, L. Rifas, S.R. Rittling, D.T. Denhardt, K.A. Hruska, Osteopontin deficiency produces osteoclast dysfunction due to reduced CD44 surface expression, Mol. Biol. Cell 14 (2003) 173–189, https://doi.org/10.1091/mbc.E02-06-0354.

[39] W. Huang, B. Carlsen, G. Rudkin, M. Berry, K. Ishida, D.T. Yamaguchi, T.A. Miller, Osteopontin is a negative regulator of proliferation and differentiation in MC3T3-E1 pre-osteoblastic cells, Bone 34 (2004) 799–808, https://doi.org/10.1016/j.bone.2003.11.027.

[40] B. Hoac, V. Nelea, W. Jiang, M.T. Kaartinen, M.D. McKee, Mineralization-inhibiting effects of transglutaminase-crosslinked polymeric osteopontin, Bone 101 (2017) 37–48, https://doi.org/10.1016/j.bone.2017.04.007.